small structures
www.small-structures.com

A New Insight of Anti-Solvent Electrolytes for Aqueous Zinc-Ion Batteries by Molecular Modeling

*Yilong Zhu, Junnan Hao, Yan Huang, and Yan Jiao**

Aqueous zinc-ion batteries (AZIBs) have attracted wide attention for large-scale energy storage. However, the practical application of AZIBs is limited by the poor reversibility of Zn anodes. Recently, a strategy of adding low-cost anti-solvent to electrolytes is proposed experimentally, which can improve Zn reversibility therefore the AZIBs performance. Nevertheless, the mechanism of the strategy remains elusive, especially how the Zn reversibility is improved and why various anti-solvents perform differently. Herein, atomic-level insight into the mechanism, is provided, by modeling $ZnSO_4$ electrolytes with different anti-solvents, that is, methanol and ethanol. Through molecular dynamics simulations and density-functional theory calculations, how anti-solvents impact Zn^{2+} solvation sheath and water activity is explored. It is suggested in the results that methanol promotes Zn reversibility for two reasons. First, methanol can modify the Zn^{2+} solvation sheath to reduce the energy barrier for Zn^{2+} de-solvation. Second, methanol can form H-bond with water molecules to suppress H_2 evolution. Based on the new atomic level insight, herein, the practical universality of the anti-solvent strategy is confirmed in other aqueous batteries for developing more effective anti-solvents.

1. Introduction

The demand for renewable energy has spawned a potential market for high-performance energy storage devices in recent years.[1] Compared to nonaqueous electrolytes, a battery technique based on aqueous electrolytes features low flame risk and high ionic conductivity, enabling aqueous batteries with high safety and high-rate capability.[1,2] Among different types of aqueous batteries, rechargeable aqueous Zn-ion batteries (AZIBs) have been widely regarded as a promising alternative to Li-ion batteries for large-scale energy storage, because the metallic Zn anode has good compatibility with aqueous electrolytes and a high theoretical anode capacity (820 mAh g^{-1}).[3]

One of the bottlenecks of AZIBs is the low Coulombic efficiency (CE) of Zn anodes caused by irreversible side reactions of hydrogen evolution reaction (HER) and the Zn dendrite growth during the charge–discharge process.[4] Although the Zn metal has a high overpotential against HER, the competing hydrogen production inevitably occurs within aqueous batteries.[5] A significant impact from HER is the increased hydroxide ion (OH^-) concentration near the Zn electrode surface.[6] The elevated OH^- concentration in the system will corrode the Zn electrode to form an inactive $Zn_4SO_4(OH)_6{\cdot}xH_2O$ by-product, which aggravates the Zn dendrite growth by hindering the ion/electron diffusion and further reduces the reversibility of Zn anodes.[6a,b,7]

To address HER and Zn dendrite growth issues relevant to Zn anodes, a variety of electrolyte strategies have been proposed, such as increasing salt concentration and adding organic additives.[8] Increasing the salt concentration in the electrolyte could improve the reversibility of Zn^{2+} by reducing the solvation effect of the solution system.[8b] For example, a highly concentrated aqueous electrolyte composed of 20 M bis(trifluoromethane) sulfonimide lithium salt (LiTFSI) and 1 M $Zn(TFSI)_2$ was proposed.[8c] However, the price of the proposed electrolyte with high salt concentration is high, prohibiting its large-scale applications in aqueous batteries.[9] Another strategy was introducing organic additives to the electrolyte, such as triethyl phosphate (TEP) and dimethyl sulfoxide (DMSO). However, these organic solvents not only increase the viscosity of electrolytes, but also increase the risk of flammability, compromising the advantages of aqueous batteries.[10] Very recently, an anti-solvent strategy by adding methanol to $ZnSO_4$ electrolytes in AZIBs was proposed and demonstrated successful in addressing HER and dendrite growth issues.[11] However, the fundamental-level understanding is not sufficient to explain how the anti-solvent works and why various anti-solvents behave differently. Therefore, it is highly desirable to investigate the underlying mechanism of how anti-solvent functions in the aqueous electrolyte on a molecular level. This fundamental understanding is critical to evaluate the feasibility of the proposed anti-solvent strategy.

Y. Zhu, J. Hao, Y. Jiao
School of Chemical Engineering and Advanced Materials
The University of Adelaide
Adelaide 5005, Australia
E-mail: yan.jiao@adelaide.edu.au

Y. Huang
School of Materials Science and Engineering
Harbin Institute of Technology
Shenzhen 518055, P. R. China

The ORCID identification number(s) for the author(s) of this article can be found under https://doi.org/10.1002/sstr.202200270.

DOI: 10.1002/sstr.202200270

Herein, we investigate two common mono-alcohols (methanol and ethanol) as low-cost anti-solvents to the $ZnSO_4$ electrolyte in AZIBs. The selection of the two mono-alcohols is based on their small molecular size and high dielectric constant.[12] We first perform experiments to demonstrate the different physical phenomena of $ZnSO_4$ electrolyte after adding two mono-alcohols, including their physical appearance, the suppression of HER, and the change in spectroscopy measurements, which reflect solvation structure. Then, molecular dynamics (MD) simulation and density-functional theory (DFT) calculation are further performed to study the Zn^{2+} solvation structure and water activity caused by anti-solvents addition. Our molecular modeling demonstrates that both methanol and ethanol as anti-solvents could form H-bond with free water and reduce water activity. The major difference is that methanol could reshape Zn^{2+} solvation structure by entering the Zn^{2+} solvation sheath, which promotes the Zn^{2+} reversibility. In comparison, ethanol could not regulate the Zn^{2+} solvation sheath due to lower interaction energy and ion–dipole interaction energy. In the last part, we demonstrate that this anti-solvent strategy can be extended to other aqueous electrolytes (such as Li_2SO_4 and Na_2SO_4), which indicates the practical universality of anti-solvent strategy in other aqueous battery systems.

2. Results and Discussion

We first experimentally prepared two anti-solvent electrolytes, by adding methanol and ethanol to 2 M $ZnSO_4$. **Figure 1**a,b insets show that adding methanol and ethanol to the $ZnSO_4$ electrolyte results in different phenomena, despite both of them are mono-alcohols. Figure 1a inset shows that methanol and $ZnSO_4$ electrolyte could form a homogeneous phase when less methanol is added (less than or equal to 55% volume ratio of methanol). Since $ZnSO_4$ is insoluble in alcohol, Zn^{2+} and SO_4^{2-} in solution would dissolve and recrystallize when adding high volume ratio of methanol. The recrystallization shows that the addition of anti-solvent reduces the solubility of $ZnSO_4$, which indicates that the micro-structure of Zn^{2+} can only be adjusted to a certain extent by controlling the ratio of methanol.

Similarly, the $ZnSO_4$ electrolyte could form a homogeneous mixture with ethanol when its volume ratio is less than 25% (Figure 1b inset). Different from methanol, delamination of the solution occurs when the volume ratio of ethanol is reached 35%, in which the solution is first separated into two layers due to the difference in polarity between ethanol and high-concentration solutions.[13] Our further analysis confirms that after adding an extensive amount of ethanol, the upper layer (mainly ethanol) contains a lower concentration of $ZnSO_4$, while

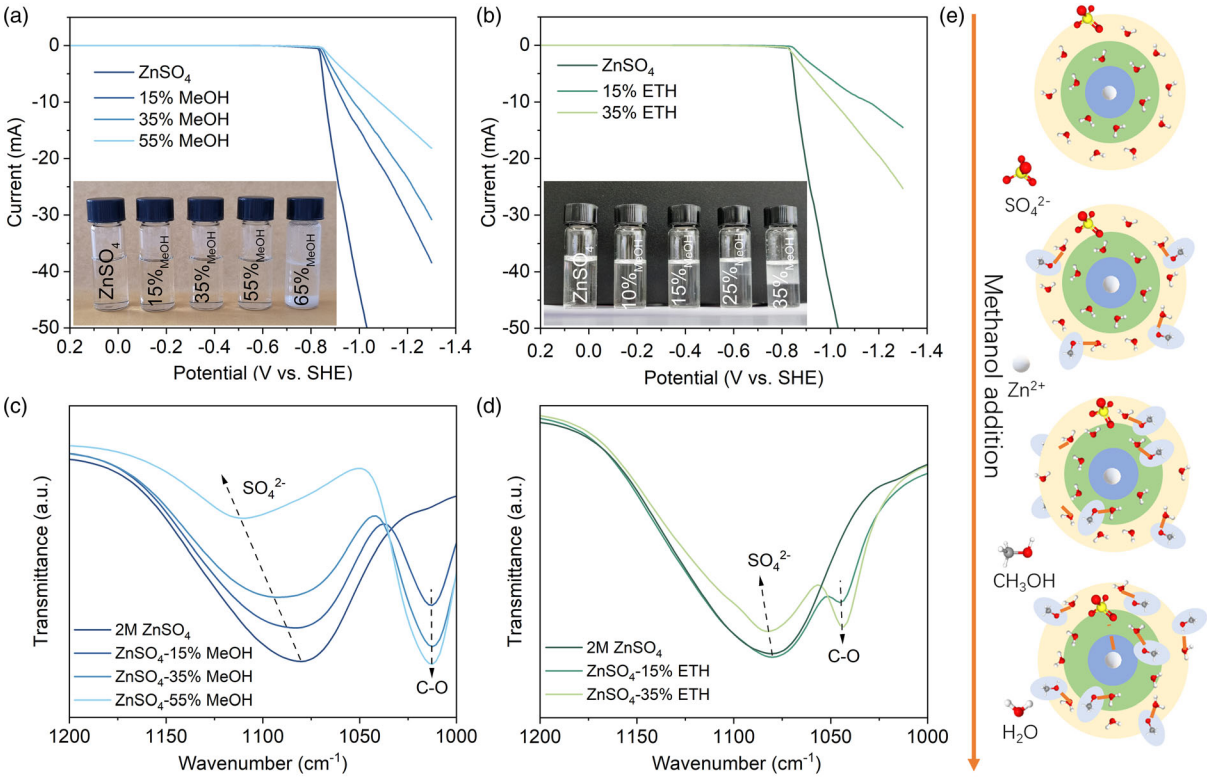

Figure 1. Hydrogen evolution and solvation structure change of electrolyte with anti-solvent. linear sweep voltammetry (LSV) of electrolyte with a) methanol and b) ethanol as anti-solvent. LSV for pure $ZnSO_4$ electrolyte are included for comparison purposes. Insets are the electrolyte solutions after adding various amounts of anti-solvent. Please note $ZnSO_4$ solute is recrystallized after adding 55% volume ratio of methanol, and $ZnSO_4$ electrolyte is stratified after adding 35% volume ratio of ethanol. Fourier-transform infrared (FTIR) spectra of electrolyte with c) methanol and d) ethanol as anti-solvent. The performance of pure $ZnSO_4$ electrolyte is included for comparison purposes. e) Schematic diagram of the change of Zn^{2+} solvation sheath along with the methanol addition.

the lower layer (mainly water) contains a higher concentration of $ZnSO_4$ (Table S1, Supporting Information). In addition, both anti-solvents addition would also affect the Zn^{2+} ionic conductivity, as presented in Figure S1, Supporting Information. The influence of methanol on Zn^{2+} ionic conductivity is greater than that of ethanol, indicating that ethanol has stronger hydrophobicity and lower solubility than methanol.

To evaluate the effect of anti-solvents on water activity, the linear sweep voltammetry (LSV) curves were measured (Figure 1a,b). Under the same cutoff voltage, $ZnSO_4$ electrolytes with different volume ratios of anti-solvents show lower current than pristine $ZnSO_4$ electrolyte. Such phenomenon indicates that both methanol and ethanol could effectively suppress the H_2 evolution. With the increase of methanol concentration, hydrogen evolution was suppressed (Figure 1a). Although the addition of ethanol can also inhibit hydrogen evolution, the reduction of hydrogen production is significantly lower than that by methanol at the same concentration. In addition, higher concentration (35%) of ethanol shows lower hydrogen evolution activity than lower ethanol concentration (15%), as shown in Figure 1b. As shown in Figure S2, Supporting Information, the 2 M $ZnSO_4$ electrolyte undergoes a significant current response at −1.7 V versus SHE, which indicates that the oxygen evolution starts. Then, the current response rises up to 45.7 mA at 2.0 V versus SHE. In comparison, the $ZnSO_4$ electrolyte after adding anti–solvents has lower values of current response: 3.1 mA of adding 55% methanol and 14.6 mA of adding 35% ethanol. This phenomenon indicates both methanol and ethanol could effectively suppress the O_2 evolution. In addition, methanol (55%) exhibits a lower oxygen evolution activity than ethanol (35%). The outcomes demonstrate that methanol is superior to ethanol in its ability to suppress hydrogen evolution.

To evaluate the addition of anti-solvents on solvation structure, we further obtained Fourier-transform infrared (FTIR) spectroscopy curves for different samples. As shown in Figure 1c, for pure $ZnSO_4$ electrolyte, the peak located at 1079.4 cm^{-1} could be ascribed to the vibration of SO_4^{2-}. Compared with pure $ZnSO_4$ electrolyte, the SO_4^{2-} peak shifted to higher wavenumber after adding different volume ratios of methanol. For example, when 55% methanol is added, the frequency for SO_4^{2-} is 1114.6 cm^{-1}. This change in SO_4^{2-} wavenumber suggests a stronger binding between SO_4^{2-} and Zn^{2+} in a modified Zn^{2+} solvation structure. In comparison, when ethanol is added as anti-solvent, the vibration peak of SO_4^{2-} shows slight change, suggesting that ethanol has less impact on Zn^{2+} solvation structure (Figure 1d). At the same time, the weakening of the SO_4^{2-} signal is due to the fact that with the increase of the proportion of alcohol added, the proportion of SO_4^{2-} decreases in the same volume of the solution. The peak located at 1012.5 cm^{-1} is the stretching vibration of the strongly C—O bond of methanol added to $ZnSO_4$ solutions (Figure 1c). Similarly, the peak located at 1043.3 cm^{-1} is the stretching vibration of the C—O bond of ethanol adding in $ZnSO_4$ solutions (Figure 1d). In addition, the intensity of C—O vibration peak increases with the volume ratio of methanol increases. Based on the change in Zn^{2+} and SO_4^{2-} binding, how methanol affects the Zn^{2+} solvation structure in $ZnSO_4$ electrolyte is proposed in Figure 1e. Before adding methanol, Zn^{2+} shows a stable double-layer solvated structure in aqueous $ZnSO_4$ electrolyte. The structure of outer and inner sheath of Zn^{2+}gradually changes with more methanol adding into the solution, which disrupts the coordination balance of water and Zn^{2+} in the solvation sheath. Outside the Zn^{2+} solvation sheath, methanol can attract free water as it forms H-bond with water molecule.

The reversibility of the Zn chemistry was investigated by performing plating/stripping measurements on Zn/Cu coin cells at 2 mA cm^{-2} and 1 mAh cm^{-2}. As shown in Figure S3, Supporting Information, the Zn/Cu cell with pure 2 M $ZnSO_4$ electrolyte failed after the 81st cycle. In addition, the value of CE fluctuated in subsequent cycles, which was mainly caused by dendritic deposition, H_2 evolution, and $Zn_4SO_4(OH)_6{\cdot}xH_2O$ by-product formation.[14] In contrast, the Zn/Cu cell with the addition of anti-solvents exhibited high CEs in the first 10 cycles and remained stable for approximately 500 cycles, obtaining a high average value of 99.2%. Similarly, 35% ethanol achieved an average CE value of 99.1%. Experiments show that the addition of anti-solvent methanol (55%) and ethanol (35%) could significantly improve CE and cycling life of Zn electrodes.

To further investigate how methanol and ethanol as anti-solvents affect the water activity and Zn solvation structure, MD simulations were conducted. More details of the MD simulation could be found in Experimental Section and Supporting Information. Snapshots of equilibrated system are shown in **Figure 2**a (pristine $ZnSO_4$ electrolyte), Figure 2d (55% methanol), and Figure 2g (35% ethanol). The enlarged local structure surrounding zinc ions are shown in Figure 2b,e,h, correspondingly. Figure 2b (pristine $ZnSO_4$ electrolyte) shows that water molecules and SO_4^{2-} enclose the Zn^{2+} ion. Figure 2e (55% methanol) shows that one methanol molecule occupies the position of the original coordinated water molecules in the Zn^{2+} solvation structure. However, Figure 2h (35% ethanol) shows that ethanol molecules barely occupy the position of the original coordinated water molecules in the Zn^{2+} solvation structure.

The changes of Zn^{2+} solvation structure after adding anti-solvents are further confirmed by radial distribution function (RDF; i.e., $g(r)$) and coordination number (N_{Coor}) of Zn^{2+} with the oxygen in water or anti-solvents. The last 5 ns within equilibrium simulations were used. Figure 2c suggests that there are two solvation sheaths for Zn^{2+} in pure $ZnSO_4$ electrolyte (black line). The first solvation sheath locates at about 2.1 Å from Zn^{2+}, and the second sheath is at around 4.3 Å. For the first solvation sheath of Zn^{2+} in pure $ZnSO_4$ electrolyte, the water coordination number is 4. This is less than the reported coordination number of 6, due to that SO_4^{2-} also coordinates with Zn^{2+}.[14] Figure S4, Supporting Information, reports coordination number of 6 in the solvation sheath of pure Zn^{2+} solution system without SO_4^{2-}, which aligns with reported values. When methanol is added to the $ZnSO_4$ solution (Figure 2f), there is a peak (black dotted line) in the RDF of methanol at the first water sheath, showing that methanol can enter the first water sheath. Figure 5 shows the RDF for different methanol ratio; further confirming methanol can enter the solvation sheath. In addition, more methanol could enter the solvation sheath with higher volume ratio of methanol. In comparison, there is no peak (black dotted line) in the RDF of ethanol (Figure 2i) at the first water solvation sheath, indicating that no ethanol appears in first Zn^{2+} solvation sheath. Overall, our results suggest that methanol as anti-solvent can disturb

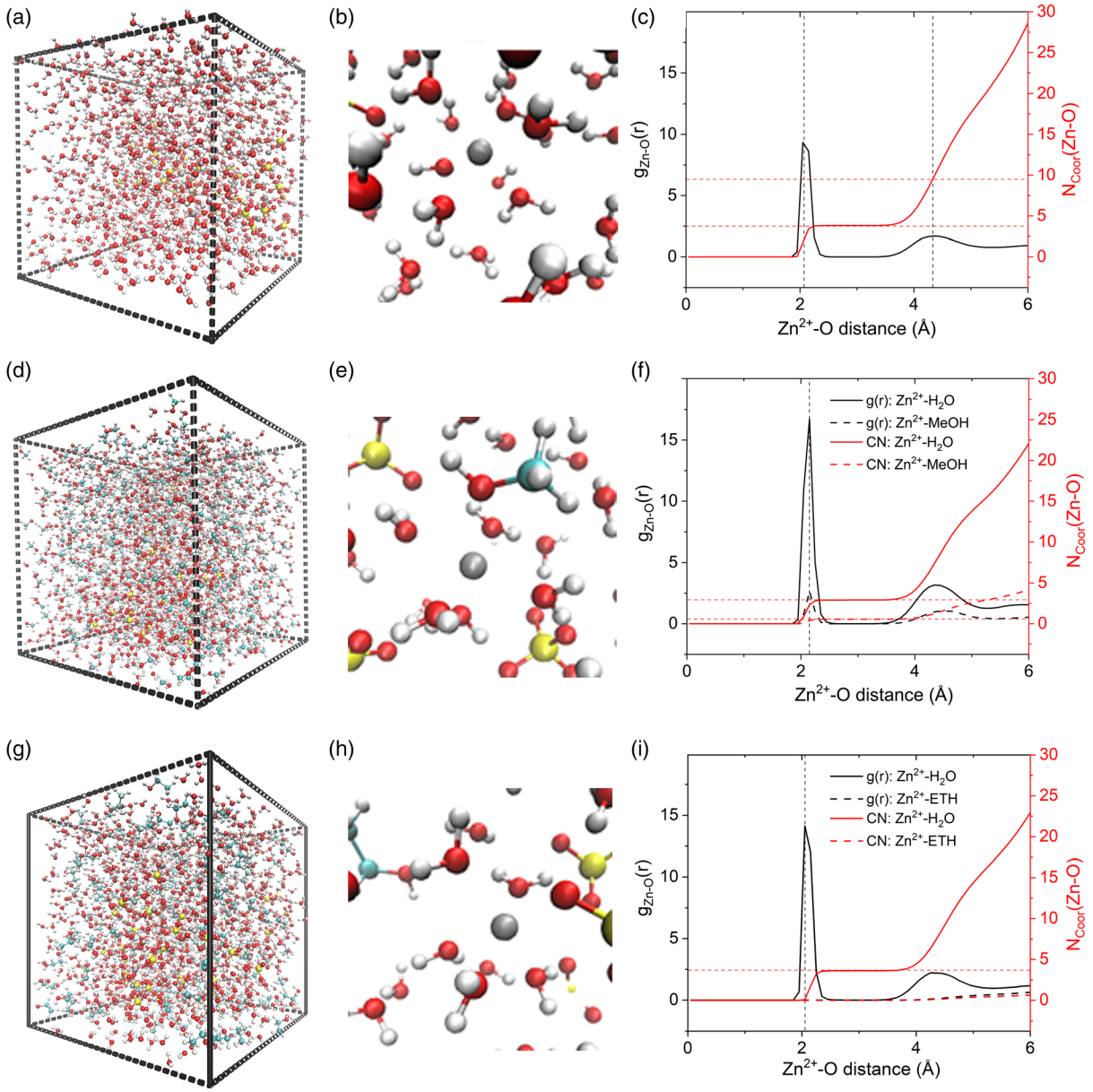

Figure 2. Atomic configuration and local density of various electrolytes at the last 5 ns of the equilibrium simulations. Snapshot of a) 2 M $ZnSO_4$ electrolyte, d) 2 M $ZnSO_4$ electrolyte with 55% volume ratio of methanol, and g) 2 M $ZnSO_4$ electrolyte with 35% volume ratio of ethanol. b,e,h) Their local enlarged structures are shown, correspondingly. RDF and coordination number of zinc ion and oxygen in c) pure $ZnSO_4$ solution, f) $ZnSO_4$ solution with 55% volume ratio of methanol, and i) $ZnSO_4$ solution with 35% volume ratio of ethanol. Color code: red, O; white, H; yellow, S; cyan, C; grey, Zn.

the water sheath around Zn^{2+}, which contributes to the high Zn^{2+} transmission.

To explore the fundamental reason why methanol and ethanol as anti-solvent have different impacts on the Zn^{2+}–water solvation sheath, we performed DFT calculations to perform electrostatic potential (ESP) analysis on three systems, including the pure $ZnSO_4$ electrolyte (Zn^{2+} with 6 waters), $ZnSO_4$ electrolyte with methanol (Zn^{2+} with 5 waters and 1 methanol), and $ZnSO_4$ electrolyte with ethanol (Zn^{2+} with 5 waters and one ethanol). As shown in **Figure 3**a, the maximum ESP of the solvation sheath of Zn^{2+} with 6 water molecules (Zn^{2+}–$6H_2O$) is 248 Kcal mol^{-1}. When the methanol molecule replaces a water molecule (Figure 3b), the maximum ESP value decreases to 224 Kcal mol^{-1} (Zn^{2+}–$5H_2O$–CH_3OH). This indicates that the addition of methanol can reduce the electrostatic repulsion between Zn^{2+} solvation sheaths, leading to a low-energy barrier for Zn^{2+} de-solvation and rapid transmission of Zn ions.[14a] In addition, the low ESP value of Zn^{2+}–$5H_2O$–CH_3OH weakens the obstructed effect of the water sheath on Zn^{2+}.[7a] In contrast, the ESP value near the ethanol molecule is basically unchanged from the original water molecule (minimum 132 Kcal mol^{-1}; maximum 253 Kcal mol^{-1}). It indicates that the ethanol molecule

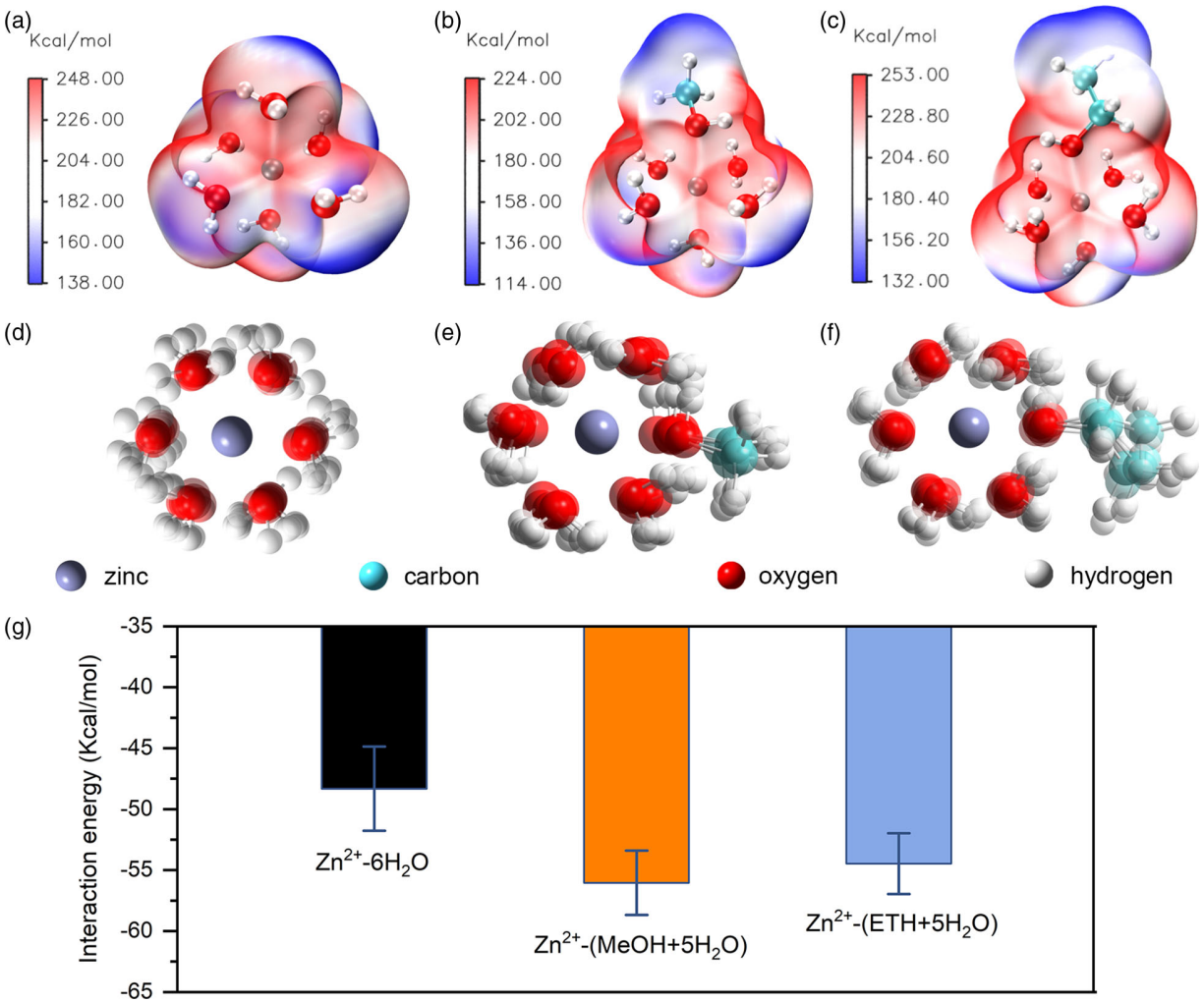

Figure 3. Energy changes of different molecule structures in the first solvation sheath of Zn^{2+}. Electrostatic potential (ESP) maps of a) the original Zn^{2+}–H_2O system, b) the Zn^{2+}–$5H_2O$–$1CH_3OH$ system, c) the Zn^{2+}–$5H_2O$–$1CH_3CH_2OH$ system. Structures explored to obtain interaction energy between Zn^{2+} and first solvation sheath: d) Zn^{2+}–H_2O; e) Zn^{2+}–$5H_2O$–$1CH_3OH$; f) Zn^{2+}–$5H_2O$–$1CH_3CH_2OH$. g) Interaction energies of three solvation systems (Zn^{2+}–H_2O, Zn^{2+}–$5H_2O$–$1CH_3OH$, and Zn^{2+}–$5H_2O$–$1CH_3CH_2OH$) with error bar.

has little effect on reducing the energy barrier for Zn^{2+} de-solvation and the transmission process of Zn^{2+}. We would suggest this is mainly because the dielectric coefficient (24.5) of ethanol is lower than that of methanol (37.2).[12] In addition, ethanol has a larger molecular size (0.43 nm) and lower polarity (0.654) than methanol (0.36 nm and 0.762). Therefore, the larger ethanol possesses higher energy barrier when inserting the Zn^{2+} solvation structure.[15] Overall, compared to methanol, it is more challenging for ethanol molecules to reshape the Zn^{2+} solvation sheath and further affect the Zn^{2+} solvation balance.

We further examined the interaction energy between Zn^{2+} and the surrounding solvation environment. As shown in Figure 3d–f, we optimized six structures for each solvation (pure water, with methanol, with ethanol) to explore all possibilities. For all the optimized structures, all oxygen atoms from water and alcohol are oriented toward Zn^{2+} (Figure 3e,f). This is due to the electrostatic energy between ion (Zn^{2+}) and polarized molecular (water or anti-solvents), which is relevant to the properties of the solvated structure. The interaction energy for each system was obtained according to the Experimental Section and summarized in Figure 3g. Generally speaking, methanol shows stronger interaction with the Zn^{2+} solvation sheath as suggested by the low interaction energy, compared with ethanol. Therefore, methanol can enter the solvation sheath, supporting our observation in the MD part.

Combining the findings, we conclude that methanol can re-regulate the solvation structure in the electrolyte. Because of the electrostatic repulsion and energy barrier both decrease with the addition of methanol, the binding between SO_4^{2-} and Zn^{2+} is strengthened. Such strengthened binding leads to the blue shift of SO_4^{2-} peak in the FTIR spectroscopy in Figure 1c. On the contrary, ethanol has little effect on the solvation structure with the bare contribution to the binding between SO_4^{2-} and Zn^{2+} shown in Figure 1d.

Apart from the effects on the Zn^{2+} solvation, anti-solvents also impact the H_2 evolution reaction within the $ZnSO_4$ electrolyte, as

suggested by the experimental results in Figure 1a,b. In this regard, we performed further H-bond analyses based on the MD simulations. **Figure 4**a shows the H-bond energies of H_2O–H_2O, H_2O–methanol, and H_2O–ethanol molecules. It shows that both methanol and ethanol with water molecule have higher H-bond energies (−5.71 and −5.95 Kcal mol^{-1}) than the energy between water molecules. The difference in hydrogen bond energy indicates that the introduction of methanol and ethanol might influence the original H-bond network between water molecules and reduce the water activity.

We further explored the number of hydrogen bonds in different solvation. The criterion for hydrogen bond was based on geometric consideration (Figure 4b). If the structure of O–H···O falls within the radius(R)–angle(β) range of less than 3.5 Å–40° in the water cluster, a hydrogen bond is formed.[16] Figure S6, Supporting Information, shows the H-bond length within three solvation structures. It shows that ethanol–H_2O has the shortest H-bond length of 1.875 Å, and H_2O–H_2O has the longest H-bond length of 1.917 Å. This proves that ethanol has higher H-bond strength to form H-bond with water molecules.[17] Figure 4c shows the average number of H-bond per H_2O in different electrolytes. In pure $ZnSO_4$ solution, the number of average H-bond per water in pure $ZnSO_4$ solution is about 2.85. With methanol addition to the $ZnSO_4$ solution, the H-bond number gradually reduces to 2.03, which causes a 28% reduction compared to the pure $ZnSO_4$ solution. The addition of ethanol can also inhibit water activity with the H-bond number that decreases from 2.85 to 2.53.

Figure 4d–f gives more detail about the H-bond changes with simulation time in different electrolytes. For pristine water electrolyte (Figure 4d), the number of H-bond in the system remains stable at around 2.85 after minimization. With the addition of methanol, the number of H-bond decreases to nearly 2.03. Similarly, with the addition of ethanol, the number of H-bond decreases to approximately 2.53. This confirms that both methanol and ethanol can reduce the H-bond between water molecules. With the addition of anti-solvents, there are less hydrogen bonds between water molecules. Therefore, the order of the original water–water H-bond network is disrupted, which effectively reduces the activity of water molecules, thereby suppressing the HER.[18] However, there is a difference of hydrogen number reduction after adding the same 35% volume ratio of methanol (2.21) and ethanol (2.53) as anti-solvents. In addition, the hydrogen bond number change after adding maximum possible anti-solvents is significantly different. The 35% volume ratio of ethanol in $ZnSO_4$ solution (Figure 4f) forms less H-bond (around 0.7) than 55% volume ratio methanol of $ZnSO_4$ solution (around 1.8, Figure 4e). Our simulation confirms that methanol can inhibit water activity more effectively than ethanol, and these outcomes are also consistent with the experimental results (Figure 1a,b). To summarize, methanol can both disturb the Zn^{2+} first solvation structure and inhibit water activity, having higher performance than ethanol as an anti-solvent.

Our previous simulation results suggest that the anti-solvent strategy is based on the change of Zn^{2+} solvation sheath and water activity. Based on this, such a strategy should be able to be applied to other similar aqueous electrolytes, such as Li_2SO_4 and Na_2SO_4. To verify this that anti-solvent strategy has universality, methanol was added to the Li_2SO_4 and Na_2SO_4 aqueous electrolytes with different proportions. Results (**Figure 5**a) show that the Li_2SO_4 solution was recrystallized when the ratio of methanol was added to over 35%.

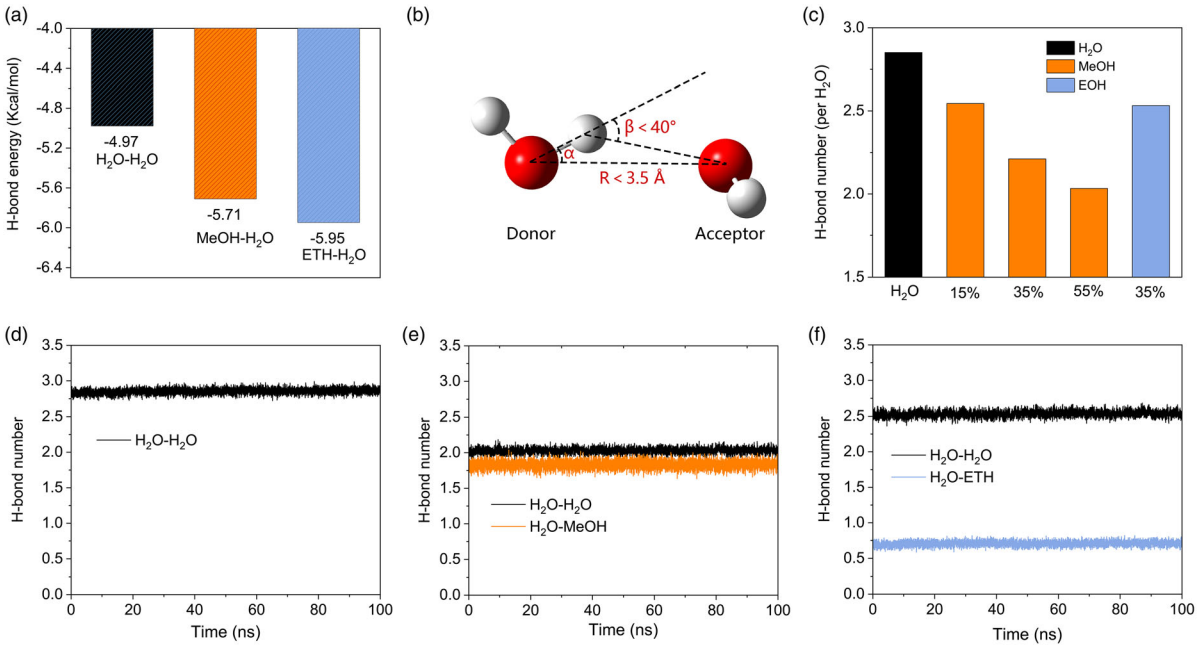

Figure 4. H-bond changes of different electrolytes. a) The H-bond energies of H_2O–H_2O, H_2O–methanol, and H_2O–ethanol. b) The criterion for judging H-bond for the analysis of molecular dynamics (MD) trajectory. c) The H-bond number per water molecule in various solutions for the 100 ns (after equilibrium) of the MD simulation. H-bond changes with simulation time in d) pure $ZnSO_4$ solution, e) $ZnSO_4$ solution with 55% volume ratio of methanol, and f) $ZnSO_4$ solution with 35% volume ratio of ethanol.

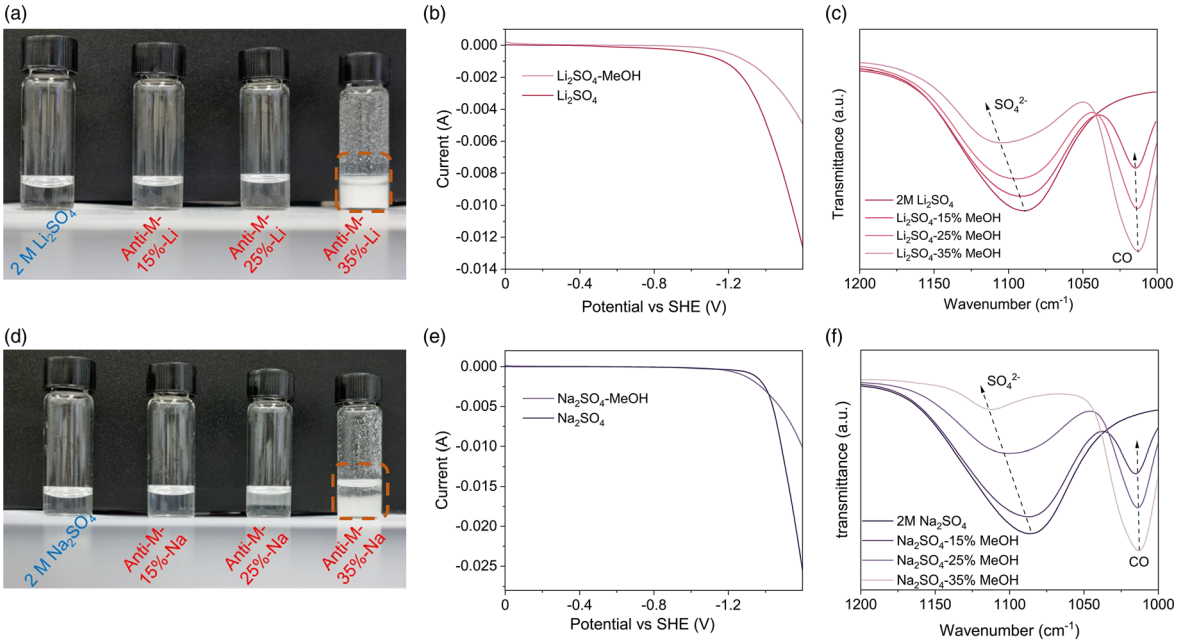

Figure 5. Methanol as anti-solvent for Li_2SO_4 and Na_2SO_4 electrolytes. a) Methanol-based Li_2SO_4 solution, which is recrystallized when adding over 35% volume ratio of methanol. b) LSV curves and c) FTIR spectra of Li_2SO_4 with and without 35% methanol. d) Methanol-based Na_2SO_4 solution, showing that solution stratified when adding over 25% volume ratio of methanol and Na_2SO_4 recrystallized over 35% volume ratio of methanol. e) LSV curves and f) FTIR spectra of Na_2SO_4 solution with and without 25% methanol.

Similarly, the Na_2SO_4 solution was also stratified when the ratio of methanol was added to over 25%, and recrystallization occurs when the ratio of methanol is more than 35% (Figure 5d). This suggests that similar to the $ZnSO_4$ electrolyte, the methanol can reshape the Li^+ and Na^+ solvation structure in each electrolyte by forming H-bond with free water and coordinated water.

To demonstrate that methanol can alter water activity in Li_2SO_4 and Na_2SO_4 electrolytes, the LSV curves were collected. The results (Figure 5b) show that under the same cutoff voltage, the Li_2SO_4 electrolyte with a 35% volume ratio of methanol has a lower current than the Li_2SO_4 electrolyte without methanol, indicating that the H_2 evolution is effectively suppressed. This confirms that the addition of methanol could reduce the water activity of the solution, which helps to enhance the electrochemical performance of anti-solvent-based batteries. Moreover, adding methanol to the Na_2SO_4 electrolyte shows similar results according to the aforementioned LSV curves (Figure 5e). To evaluate the addition of anti-solvents to solvation structure, FTIR spectrum was obtained. As shown in Figure 5c, the peak locates at 1085.7 cm^{-1} could be ascribed to the vibration of SO_4^{2-} in the pure Li_2SO_4 solution. Compared with pure $ZnSO_4$ solution, the SO_4^{2-} wavenumber peak shifts to a higher wavenumber after adding different volume ratios of methanol. For example, when 35% methanol is added, the frequency for SO_4^{2-} is 1113.2 cm^{-1}, suggesting that the frequency of SO_4^{2-} is decreased. Similarly, adding methanol to the Na_2SO_4 electrolyte shows similar results according to the aforementioned FTIR curves (Figure 5f). The vibration peak of SO_4^{2-} s wavenumber peak shifts from 1089.6 to 1107.3 cm^{-1} (pure Na_2SO_4 solution to Na_2SO_4 solution with the addition of 35% methanol, respectively) after adding the different volume ratios of methanol. The aforementioned FTIR results confirm that methanol also has a modified effect on Li^{2+} and Na^+ solvation structure. In short, these results indicate that in addition to being effective in aqueous zinc electrolytes, methanol can also be applied to Li/Na-based aqueous electrolytes as a low-cost anti-solvent to solve the common problem of H_2 evolution.

3. Conclusion

In summary, we provided atomic-level insight to an economical and effective anti-solvent strategy. Our simulation results show that methanol could modify the Zn^{2+} solvation sheath, as well as reducing the coordination number of water molecules around Zn^{2+}. The fundamental reason for methanol modifying the water sheath could be explained by the reduced electrostatic repulsion between Zn^{2+} cations and methanol, and the increased interaction between Zn^{2+} cations and methanol. H-bond analysis results show that in the $ZnSO_4$ solution after adding monoalcohols, the H-bond number between water molecules is decreased, which consequently suppresses the H_2 evolution of aqueous batteries. This research illustrates its universality by applying to other types of aqueous batteries to effectively resolve the general problem of water-induced H_2 evolution.

4. Experimental Section

Experiment: All sulfates (including $ZnSO_4$ (>99.5%), Na_2SO_4 (>99.5%), and Li_2SO_4 (>99.5%)) and monohydric alcohols—methanol (anhydrous, 99.8%) and ethanol (anhydrous, >99.5%)—were purchased from Sigma–Aldrich Chemical Co. Deionized water was used to prepare all

aqueous electrolytes. For the $ZnSO_4$ solution configuration, the methanol was added to the prepared 2 M $ZnSO_4$ solution (the methanol concentration ranges from 15% to 55% volume ratio). Similarly, in the $ZnSO_4$ solution with ethanol configuration, the concentration was from 10% to 35% (volume ratio). Then, for the 2 M Na_2SO_4 solution configuration, the concentration of methanol added was from 15% to 35% (volume ratio), expressed with Anti-M–v%–Na. For the 2 M Li_2SO_4 solution configuration, the methanol concentration ranged from 15% to 35% (volume ratio), expressed as Anti-M–v%–Li.

LSV curves of $ZnSO_4$, Na_2SO_4, and Li_2SO_4 were collected using a three-electrode system. The Ag/AgCl electrode was used as the reference electrode, of which potential E_0 against standard hydrogen electrode (SHE) is +0.2225 V.[19] The LSV results have been converted to V versus SHE. And stainless steel was used as working electrode and counter electrode. The test was performed on an electrochemical working station CHI 760E within a voltage range from 0 to −1.6 V with a scan rate of 1 mV s^{-1}.

FTIR spectra of the Zn electrode and polished Zn foil were acquired in duplicate in the range 4000–600 cm^{-1} using a PerkinElmer Frontier FTIR spectrometer (PerkinElmer, Boston, MA, USA) with a resolution of 2 cm^{-1} and averaging 8 scans for each spectrum.

MD Simulation: MD simulations were performed on aqueous electrolytes added with $ZnSO_4$ salt with different anti-solvent volume ratios. Simulations were carried out using the NAnoscale Molecular Dynamics (NAMD) package to investigate the solvation structure of electrolytes.[20] The solution model contained different numbers of $ZnSO_4$, water molecules, and anti-solvent molecules (**Table 1**). The size of different system cells was after 100 ps minimization and 10 ns constant temperature and pressure mumber of particles, pressure and temperature (NPT) (300 K and 1 atm; **Table 2**).

The force field parameters for methanol, ethanol, Zn^{2+}, and SO_4^{2-} were obtained from CHARMM36 force fields.[21] The TIP3P water model was employed for H_2O.[22] The time step was set to be 2 fs. The cutoff radius for vdW was 12 Å and the electrostatic interactions were 10 Å. The standard periodic boundary condition was used in all simulations. After minimization of the initial structure for 50 000 steps (100 ps), each system was heated from 100 to 300 K by performing Langevin dynamics temperature control for 0.8 ns (400 000 steps; Figure S7, Supporting Information). The systems were further relaxed for another 9.2 ns under NPT by Nosé–Hoover Langevin piston pressure control method at 1.01325 bar. After relaxation, each system was simulated for 100 ns (Figure S8, Supporting Information) under canonical ensemble (number of particles, volume and temperature [NVT]) for data collection and statistical analysis.

Table 1. Numbers of molecules in different solution models.

System	No. of water molecules	No. of $ZnSO_4$	No. of anti-solvent molecules
Additive-free $ZnSO_4$ solution	1000	36	–
15% Methanol $ZnSO_4$ solution	1000	36	79
35% Methanol $ZnSO_4$ solution	1000	36	240
55% Methanol $ZnSO_4$ solution	1000	36	545
35% Ethanol $ZnSO_4$ solution	1000	36	167

Table 2. Size of different system cells.

System	*x* [Å]	*y* [Å]	*z* [Å]
Additive-free $ZnSO_4$ solution	31.343	31.324	31.324
15% Methanol $ZnSO_4$ solution	32.847	32.887	32.808
35% Methanol $ZnSO_4$ solution	36.159	36.239	36.159
55% Methanol $ZnSO_4$ solution	40.799	40.810	40.810
35% Ethanol $ZnSO_4$ solution	36.127	36.127	36.127

DFT and Energy Calculations: DFT was used to study the surface ESP and key energy indicators as discussed later. All structures were optimized by DFT on B3LYP-D3(BJ)-mixed functional and 6-311 + G* basis sets, using Gaussian G09RevD.01 program.[23] The single-point energy calculations were performed for each optimized structure by using 6-311 + G** basis sets.[24] ESP was conducted by Multiwfn 3.8 and rendered by visual molecular dynamics (VMD).[25]

The intermolecular interaction energy was used to describe the interaction between added anti-solvent with the original solvation structure.[23] Such interaction energy ($E_{interaction}$) can be used to evaluate the easiness of solute molecules into the solvated structure.[24] The interaction energy was calculated as

$$E_{interaction} = E_{solvation-system} - E_{Zn^{2+}-5H_2O} - E_{single-molecule} + E_{BSSE} \quad (1)$$

in which $E_{solvation-system}$ refers to the total energy of three solvation systems (Zn^{2+}–$6H_2O$, Zn^{2+}–$5H_2O$–$1CH_3OH$, and Zn^{2+}–$5H_2O$–$1CH_3CH_2OH$). $E_{Zn^{2+}-5H_2O}$ refers to the energy of one zinc ion surrounded by five water molecules in the first solvation sheath after geometry optimization. $E_{single\ molecule}$ is the energy of corresponding single molecules that enters the solvation sheath (one H_2O, one methanol, or one ethanol molecule). Considering the basis set overlapping in the solvated structural system, our calculation considers basis set superposition error (BSSE) correction using the counterpoise method.[26]

Supporting Information

Supporting Information is available from the Wiley Online Library or from the author.

Acknowledgements

J.H. contributed equally to this work and should be considered co-first authors. Authors acknowledge financial support by the Australian Research Council (Grant nos. FT190100636 and DP190103472). Authors also acknowledge financial support by Project of International Science and Technology Cooperation in Guangdong Province (Grant no. 2020A0505100016). MD computations within this research were undertaken with the assistance of resources and services from the Phoenix High Performance Computing (HPC), which is supported by The University of Adelaide. DFT computations were undertaken with the assistance of resources and services from the National Computational Infrastructure (NCI), which was supported by the Australian Government.

Conflict of Interest

The authors declare no conflict of interest.

Data Availability Statement

The data that support the findings of this study are available from the corresponding author upon reasonable request.

Keywords

anti-solvent, aqueous zinc-ion batteries, free-water activity, molecular dynamics, solvation sheaths

Received: September 15, 2022
Revised: December 4, 2022
Published online:

[1] a) M. C. Lin, M. Gong, B. Lu, Y. Wu, D. Y. Wang, M. Guan, M. Angell, C. Chen, J. Yang, B. J. Hwang, *Nature* **2015**, *520*, 324; b) H. Pan, Y. Shao, P. Yan, Y. Cheng, K. S. Han, Z. Nie, C. Wang, J. Yang, X. Li, P. Bhattacharya, *Nat. Energy* **2016**, *1*, 1; c) D. Chao, W. Zhou, F. Xie, C. Ye, H. Li, M. Jaroniec, S.-Z. Qiao, *Sci. Adv.* **2020**, *6*, eaba4098.

[2] a) C. Zhong, B. Liu, J. Ding, X. Liu, Y. Zhong, Y. Li, C. Sun, X. Han, Y. Deng, N. Zhao, *Nat. Energy* **2020**, *5*, 440; b) F. Wan, Z. Niu, *Angew. Chem.* **2019**, *131*, 16508; c) J.-Y. Luo, W.-J. Cui, P. He, Y.-Y. Xia, *Nat. Chem.* **2010**, *2*, 760; d) L. Zhang, L. Chen, X. Zhou, Z. Liu, *Adv. Energy Mater.* **2015**, *5*, 1400930.

[3] a) P. He, Y. Quan, X. Xu, M. Yan, W. Yang, Q. An, L. He, L. Mai, *Small* **2017**, *13*, 1702551; b) N. Zhang, F. Cheng, J. Liu, L. Wang, X. Long, X. Liu, F. Li, J. Chen, *Nat. Commun.* **2017**, *8*, 1; c) J. Hao, L. Yuan, B. Johannessen, Y. Zhu, Y. Jiao, C. Ye, F. Xie, S. Z. Qiao, *Angew. Chem.* **2021**, *133*, 25318.

[4] a) X. Zeng, J. Hao, Z. Wang, J. Mao, Z. Guo, *Energy Storage Mater.* **2019**, *20*, 410; b) Z. Liu, T. Cui, G. Pulletikurthi, A. Lahiri, T. Carstens, M. Olschewski, F. Endres, *Angew. Chem. Int. Ed.* **2016**, *55*, 2889; c) H. Zhang, Q. Du, C. Li, X. Sun, *J. Electrochem. Soc.* **2012**, *159*, A2001; d) M. Xu, D. Ivey, Z. Xie, W. Qu, *J. Power Sources* **2015**, *283*, 358; e) J. Fu, D. U. Lee, F. M. Hassan, L. Yang, Z. Bai, M. G. Park, Z. Chen, *Adv. Mater.* **2015**, *27*, 5617; f) Y. Li, H. Dai, *Chem. Soc. Rev.* **2014**, *43*, 5257; g) S. Zhu, Y. Dai, J. Li, C. Ye, W. Zhou, R. Yu, X. Liao, J. Li, W. Zhang, W. Zong, *Sci. Bull.* **2022**, *67*, 1882; h) Y. Tan, J. Feng, L. Kang, L. Liu, F. Zhao, S. Zhao, D. J. Brett, P. R. Shearing, G. He, I. P. Parkin, *Energy Environ. Mater.* **2022**.

[5] a) Q. Zhang, J. Luan, Y. Tang, X. Ji, H. Wang, *Angew. Chem. Int. Ed.* **2020**, *59*, 13180; b) L. Ma, M. A. Schroeder, O. Borodin, T. P. Pollard, M. S. Ding, C. Wang, K. Xu, *Nat. Energy* **2020**, *5*, 743; c) Q. Yang, G. Liang, Y. Guo, Z. Liu, B. Yan, D. Wang, Z. Huang, X. Li, J. Fan, C. Zhi, *Adv. Mater.* **2019**, *31*, 1903778.

[6] a) J. Hao, X. Li, X. Zeng, D. Li, J. Mao, Z. Guo, *Energy Environ. Mater.* **2020**, *13*, 3917; b) L. Ma, S. Chen, N. Li, Z. Liu, Z. Tang, J. A. Zapien, S. Chen, J. Fan, C. Zhi, *Adv. Mater.* **2020**, *32*, 1908121; c) J. Hao, X. Li, S. Zhang, F. Yang, X. Zeng, S. Zhang, G. Bo, C. Wang, Z. Guo, *Adv. Funct. Mater.* **2020**, *30*, 2001263.

[7] a) L. Ma, T. P. Pollard, Y. Zhang, M. A. Schroeder, M. S. Ding, A. V. Cresce, R. Sun, D. R. Baker, B. A. Helms, E. J. Maginn, *Angew. Chem. Int. Ed.* **2021**, *60*, 12438; b) Z. Liu, S. Z. El Abedin, F. Endres, *Electrochem. Commun.* **2015**, *58*, 46.

[8] a) L. Yuan, J. Hao, C.-C. Kao, C. Wu, H.-K. Liu, S.-X. Dou, S.-Z. Qiao, *Energy Environ. Sci.* **2021**, *14*, 5669; b) N. Zhang, F. Cheng, Y. Liu, Q. Zhao, K. Lei, C. Chen, X. Liu, J. Chen, *J. Am. Chem. Soc.* **2016**, *138*, 12894; c) F. Wang, O. Borodin, T. Gao, X. Fan, W. Sun, F. Han, A. Faraone, J. A. Dura, K. Xu, C. Wang, *Nat. Mater.* **2018**, *17*, 543; d) Z. Hou, H. Tan, Y. Gao, M. Li, Z. Lu, B. Zhang, *J. Mater. Chem. A* **2020**, *8*, 19367; e) Z. Hou, Z. Lu, Q. Chen, B. Zhang, *Energy Storage Mater.* **2021**, *42*, 517; f) Z. Hou, B. Zhang, *EcoMat* **2022**, *4*, e12265; g) F. Zhao, Z. Jing, X. Guo, J. Li, H. Dong, Y. Tan, L. Liu, Y. Zhou, R. Owen, P. R. Shearing, *Energy Storage Mater.* **2022**, *53*, 638.

[9] J. Xie, Z. Liang, Y.-C. Lu, *Nat. Mater.* **2020**, *19*, 1006.

[10] a) L. Suo, O. Borodin, T. Gao, M. Olguin, J. Ho, X. Fan, C. Luo, C. Wang, K. Xu, *Science* **2015**, *350*, 938; b) J. F. Parker, C. N. Chervin, E. S. Nelson, D. R. Rolison, J. W. Long, *Energy Environ. Sci.* **2014**, *7*, 1117.

[11] a) J. Hao, J. Long, B. Li, X. Li, S. Zhang, F. Yang, X. Zeng, Z. Yang, W. K. Pang, Z. Guo, *Adv. Funct. Mater.* **2019**, *29*, 1903605; b) T. Zhang, F. Wang, H. Chen, L. Ji, Y. Wang, C. Li, M. B. Raschke, S. Li, *ACS Energy Lett.* **2020**, *5*, 1619.

[12] M. Mohsen-Nia, H. Amiri, B. Jazi, *J. Solution Chem.* **2010**, *39*, 701.

[13] a) W. L. Smith, *J. Chem. Educ.* **1977**, *54*, 228; b) R. Schmid, *Monatsh. Chem.* **2001**, *132*, 1295.

[14] a) N. Chang, T. Li, R. Li, S. Wang, Y. Yin, H. Zhang, X. Li, *Energy Environ. Sci.* **2020**, *13*, 3527; b) Q. Zhang, Y. Ma, Y. Lu, X. Zhou, L. Lin, L. Li, Z. Yan, Q. Zhao, K. Zhang, J. Chen, *Angew. Chem.* **2021**, *133*, 23545.

[15] Y. Tang, D. Dubbeldam, S. Tanase, *ACS Appl. Mater. Interfaces* **2019**, *11*, 41383.

[16] a) I. Brown, *Acta Crystallogr. Sect. A* **1976**, *32*, 24; b) R. Kumar, J. Schmidt, J. Skinner, *J. Chem. Phys.* **2007**, *126*, 05B611.

[17] S. J. Grabowski, *J. Phys. Org. Chem.* **2004**, *17*, 18.

[18] Q. Nian, X. Zhang, Y. Feng, S. Liu, T. Sun, S. Zheng, X. Ren, Z. Tao, D. Zhang, J. Chen, *ACS Energy Lett.* **2021**, *6*, 2174.

[19] R. Bates, J. Macaskill, *Pure Appl. Chem* **1978**, *50*, 1701.

[20] a) S. Plimpton, *J. Comput. Phys.* **1995**, *117*, 1; b) W. L. Jorgensen, D. S. Maxwell, J. Tirado-Rives, *J. Am. Chem. Soc.* **1996**, *118*, 11225; c) J.-P. Ryckaert, G. Ciccotti, H. J. Berendsen, *J. Comput. Phys.* **1977**, *23*, 327; d) R. W. Hockney, J. W. Eastwood, *Computer Simulation Using Particles*, CRC Press, Boca Raton **2021**; e) S. Nosé, *J. Chem. Phys.* **1984**, *81*, 511.

[21] J. Huang, A. D. MacKerell Jr, *J. Comput. Chem.* **2013**, *34*, 2135.

[22] P. Mark, L. Nilsson, *J. Phys. Chem. A* **2001**, *105*, 9954.

[23] a) C. Adamo, G. E. Scuseria, V. Barone, *J. Chem. Phys.* **1999**, *111*, 2889; b) F. Weigend, R. Ahlrichs, *Phys. Chem. Chem. Phys.* **2005**, *7*, 3297; c) S. F. Sousa, P. A. Fernandes, M. J. Ramos, *J. Phys. Chem. A* **2007**, *111*, 10439; d) F. De Proft, J. M. Martin, P. Geerlings, *Chem. Phys. Lett.* **1996**, *256*, 400.

[24] M. P. Andersson, P. Uvdal, *J. Phys. Chem. A* **2005**, *109*, 2937.

[25] a) T. Lu, F. Chen, *J. Comput. Chem.* **2012**, *33*, 580; b) J. Zhang, T. Lu, *Phys. Chem. Chem. Phys.* **2021**, *23*, 20323; c) W. Humphrey, A. Dalke, K. Schulten, *J. Mol. Graph. Model.* **1996**, *14*, 33.

[26] a) M. Andreev, J. J. de Pablo, A. Chremos, J. F. Douglas, *J. Phys. Chem. B* **2018**, *122*, 4029; b) J. G. March, J. P. Olsen, *Am. Political Sci. Rev.* **2006**, *100*, 675.